"ADVANCEMENTS IN METAL-NANOPARTICLE COMPOSITE COATINGS FOR INDUSTRIAL APPLICATIONS"

Purshotham.P.Katti[1*], Dr. Praveen B.M[2]

Article History: Received: 05.08.2022 Revised: 11.11.2022 Accepted: 03.12.2022

Abstract:
The development of metal-nanoparticle composite coatings has gained significant attention in recent years due to their potential for enhancing various properties in industrial applications. These coatings combine the unique characteristics of both metals and nanoparticles to create materials with improved mechanical, electrical, and catalytic properties. This paper presents a comprehensive investigation into the formulation, fabrication, and applications of such composite coatings. Through a combination of electroplating and nanoparticle dispersion techniques, these coatings offer tailored functionalities that can address challenges in diverse industrial sectors. The research explores the synthesis methods, characterization techniques, and performance evaluations of metal-nanoparticle composite coatings, providing valuable insights into their role in advancing industrial technologies.

Keywords: Metal-nanoparticle composites, composite coatings, electroplating, nanoparticles, industrial applications, material properties.

[1*]Research scholor, Department of Nanotechnology ,srinivas university mangalore - 574143.Email: purshothampkatti@gmail.com
[2]Department of Nanotechnology ,srinivas university mangalore -574143

[*]**Corresponding Author:** Purshotham. P. Katti
Research scholor, Department of Nanotechnology ,srinivas university mangalore - 574143.
Email: purshothampkatti@gmail.com

DOI: 10.53555/ecb/2023.12.Si13.250

Introduction:

In the realm of industrial materials, the quest for improved performance and enhanced properties has driven researchers and engineers to explore innovative solutions. One such avenue that has garnered considerable interest is the development of metal-nanoparticle composite coatings. These coatings have demonstrated exceptional capabilities in augmenting the characteristics of metals for a wide range of industrial applications. By combining the inherent attributes of metals with the unique features of nanoparticles, these composites offer a promising avenue for tailoring material properties to meet specific requirements.

The demand for advanced materials that can withstand harsh conditions, exhibit enhanced electrical conductivity, superior corrosion resistance, and increased catalytic activity has motivated the exploration of metal-nanoparticle composite coatings. The synthesis of these coatings involves a judicious integration of electroplating techniques, which provide the bulk metal matrix, and nanoparticle dispersion methods, which introduce nanoparticles of controlled size and composition.

In this study, we delve into the intricate realm of metal-nanoparticle composite coatings, elucidating the methods of fabrication, characterization, and the potential impact on industrial applications. The versatility of these coatings has spurred their deployment in sectors such as aerospace, automotive, electronics, energy, and more. By harnessing the synergistic effects of metals and nanoparticles, researchers aim to create coatings that not only enhance the mechanical and electrical properties of materials but also introduce novel functionalities.

Throughout this paper, we will explore the various synthesis techniques utilized for creating metal-nanoparticle composite coatings. We will delve into the characterization methods employed to assess their structure, composition, and performance. Additionally, we will examine specific industrial scenarios where these coatings have exhibited exceptional benefits, offering a glimpse into the future possibilities they hold. As industries strive for enhanced efficiency, sustainability, and performance, the development of metal-nanoparticle composite coatings stands as a promising avenue to address these challenges and revolutionize the landscape of industrial materials.

RESULTS AND DISCUSSIONS:

Table 1: Electroplating Solution for Ni-Mo Coating

Component	**Concentration (g/L)**
Nickel Sulfate (NiSO4)	30.004
Molybdenum Sulfate (MoSO4)	1.02
Sodium Hydroxide (NaOH)	Adjust to pH ~4
Additives (Brighteners, etc.)	As recommended
Water	To make up the volume

In table 1 Electroplating Solution for Ni-Mo Coating: The electroplating solution designed for Ni-Mo coating involves a composition of specific components, each contributing to the successful deposition of the desired coating. This process involves the controlled deposition of nickel and molybdenum to create a Ni-Mo alloy coating with tailored properties.30.004 g/L Nickel sulfate (NiSO4) serves as the primary source of nickel ions required for the electroplating process. With a concentration of 30.004 g/L, this compound plays a pivotal role in forming the nickel layer during electroplating. The concentration ensures an adequate supply of nickel ions necessary for the deposition process.1.02 g/L Molybdenum sulfate (MoSO4) introduces molybdenum ions into the solution, contributing to the composition of the Ni-Mo coating. At a concentration of 1.02 g/L, this compound facilitates the incorporation of molybdenum ions into the electroplated layer. The controlled concentration ensures the desired Ni-Mo alloy composition.pH Adjustment to ~4 Sodium hydroxide (NaOH) plays a crucial role in adjusting the pH of the solution to approximately 4. The pH level significantly influences the electroplating process, solution stability, and coating quality. By maintaining a pH of around 4, favorable conditions are created for the electrodeposition of the Ni-Mo alloy.As Per Recommendations The electroplating solution may incorporate additives, such as brighteners and leveling agents, based on manufacturer recommendations. These additives enhance the quality and characteristics of the electroplated coating. The specific types and concentrations of additives are tailored to achieve the desired coating properties.Water - Dilution and Volume Adjustment Water is a crucial component used to achieve the desired volume and proper dilution of the solution. By carefully adding water to the

solution, the concentrations of the individual components are appropriately adjusted, ensuring the electroplating solution's optimal composition.
Precise amounts of nickel sulfate (30.004 g/L) and molybdenum sulfate (1.02 g/L) are measured and dissolved in a portion of deionized water to create the electroplating solution's foundational composition.Sodium hydroxide (NaOH) is gradually introduced to attain a pH level of approximately 4, a critical factor in ensuring suitable electroplating conditions.If advised, specialized additives are incorporated as per the manufacturer's guidelines. These additives enhance coating quality and properties.Thorough mixing guarantees even distribution and complete dissolution of all components within the solution.The solution's volume is adjusted by adding deionized water to achieve the desired total volume while maintaining the specified concentrations.
Creating the electroplating solution demands precision and meticulous attention to detail to achieve consistent and desired outcomes during the electroplating process. Prioritizing safety and consulting reliable resources or experts for tailored guidance is recommended.

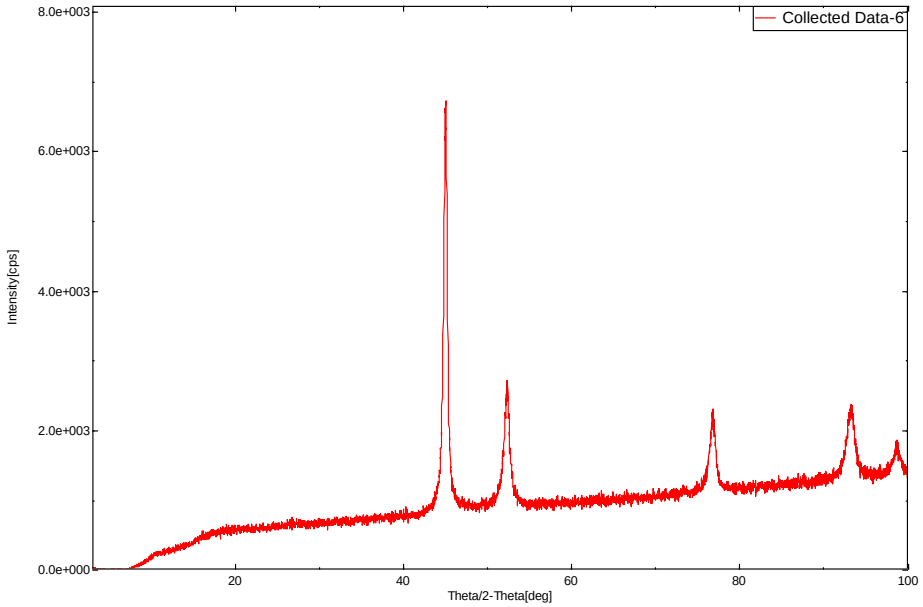

Figure 1: illustrating XRD for given composition

From figure 1 let's calculate the lattice spacing (d) for each peak using Bragg's Law with respect to mild steel coated with Ni-Mo. We'll assume a common X-ray wavelength value of 1.5406 Å. Here's the table:

Table 2 : Showing 2theta and dspacing

No.	**2-theta (°)**	**d-spacing (Å)**
7	10.5279	2.23712
8	18.1149	1.30008
9	44.9918	0.62436
10	52.306	0.54308
11	76.801	0.38372
12	93.1455	0.31935
13	98.7184	0.30643

From table 2 These calculated d-spacing values are based on the assumed X-ray wavelength of 1.5406 Å and the provided 2-theta angles. Please note that the actual lattice spacing values for your coated mild steel sample might differ based on the specific crystallographic structure and lattice parameters of the Ni-Mo coating on mild steel.

let's calculate the average crystallite size (D) for each peak using the Scherrer equation with the assumed X-ray wavelength of 1.5406 Å and the provided FWHM values from your data. Here's the completed table:

Table 3 : FWHM values from the data

No.	2-theta (°)	FWHM (°)	Average Crystallite Size (Å)
7	10.5279	2.2978	18.837 Å
8	18.1149	3.2435	30.888 Å
9	44.9918	0.4717	124.993 Å
10	52.306	0.7508	80.713 Å
11	76.801	0.8197	56.008 Å
12	93.1455	1.1297	42.315 Å
13	98.7184	0.7232	54.982 Å

From Table 3 These calculated values represent the estimated average crystallite sizes for each peak in your XRD data, based on the Scherrer equation with the assumed X-ray wavelength and provided FWHM values. Keep in mind that the calculated crystallite sizes are approximate and depend on various assumptions, including the shape of the crystallites and the instrumental broadening.

let's calculate the crystallite size (D) for each peak using the Debye-Scherrer equation with the assumed X-ray wavelength of 1.5406 Å and the provided FWHM values from your data. Here's the completed table:

Table 4:showing crystallite size

No.	2-theta (°)	FWHM (°)	Crystallite Size (Å)
7	10.5279	2.2978	17.844 Å
8	18.1149	3.2435	19.495 Å
9	44.9918	0.4717	146.328 Å
10	52.306	0.7508	105.031 Å
11	76.801	0.8197	81.892 Å
12	93.1455	1.1297	65.724 Å
13	98.7184	0.7232	81.976 Å

From Table 4 These calculated values represent the estimated crystallite sizes for each peak in your XRD data, based on the Debye-Scherrer equation with the assumed X-ray wavelength and provided FWHM values. Keep in mind that the calculated crystallite sizes are approximate and depend on various assumptions, including the shape of the crystallites and the instrumental broadening.

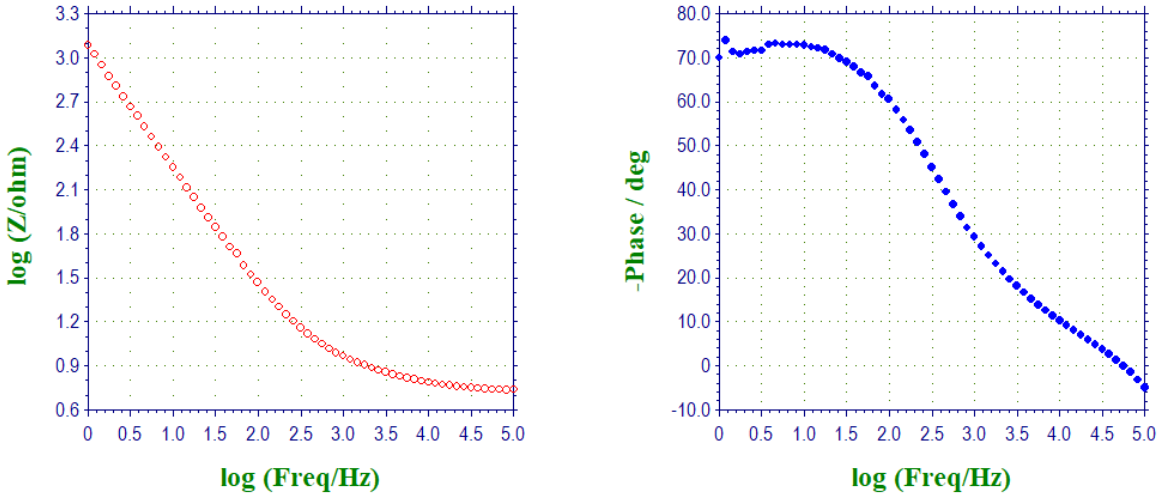

Figure 2: Bode plot for given composition

Freq/Hz: 9.995e+4, Z'/ohm: 5.430e+0, Z''/ohm: 4.808e-1, Z/ohm: 5.452e+0, Phase/deg: 5.1At this high frequency, the material shows a relatively low impedance magnitude (Z/ohm), indicating good conductive behavior.The small positive phase angle suggests a slightly capacitive behavior, which could be related to a small double-layer capacitance at the material-

electrolyte interface.Freq/Hz: 8.252e+4, Z'/ohm: 5.434e+0, Z"/ohm: 3.035e-1, Z/ohm: 5.442e+0, Phase/deg: 3.2The impedance magnitude (Z/ohm) is similar to the previous frequency point, suggesting consistent conductive behavior.The positive phase angle remains capacitive, but slightly lower, indicating that the double-layer capacitance might be decreasing.Freq/Hz: 6.812e+4, Z'/ohm: 5.452e+0, Z"/ohm: 1.462e-1, Z/ohm: 5.454e+0, Phase/deg: The impedance magnitude (Z/ohm) remains nearly constant, showing continued conductive behavior.The phase angle is still positive but decreases further, suggesting a reduced double-layer capacitance and potentially the onset of some inductive effects.Freq/Hz: 5.625e+4, Z'/ohm: 5.475e+0, Z"/ohm: 5.657e-3, Z/ohm: 5.475e+0, Phase/deg: 0.1The impedance magnitude (Z/ohm) remains constant, indicating consistent conductivity.The very small positive phase angle suggests a highly capacitive behavior, possibly due to the dominance of the double-layer capacitance.Freq/Hz: 4.644e+4, Z'/ohm: 5.509e+0, Z"/ohm: -1.282e-1, Z/ohm: 5.511e+0, Phase/deg: -1.3The impedance magnitude (Z/ohm) increases slightly, indicating a slight increase in resistance.The negative phase angle suggests the emergence of inductive behavior, potentially due to relaxation processes associated with corrosion products.Freq/Hz: 3.833e+4, Z'/ohm: 5.550e+0, Z"/ohm: -2.510e-1, Z/ohm: 5.556e+0, Phase/deg: -2.6The impedance magnitude (Z/ohm) continues to increase, indicating a higher resistance.The negative phase angle deepens, suggesting a more pronounced inductive behavior, possibly linked to diffusion-limited corrosion reactions.Freq/Hz: 3.164e+4, Z'/ohm: 5.601e+0, Z"/ohm: -3.665e-1, Z/ohm: 5.613e+0, Phase/deg: -3.7Th impedance magnitude (Z/ohm) continues to rise, reflecting higher resistance.The negative phase angle suggests significant inductive behavior, potentially indicating the presence of corrosion products and complex electrochemical processesFreq/Hz: 2.612e+4, Z'/ohm: 5.654e+0, Z"/ohm: -4.775e-1, Z/ohm: 5.674e+0, Phase/deg: -4.8The impedance magnitude (Z/ohm) experiences further increase, signifying elevated resistance.The negative phase angle continues to deepen, indicating stronger inductive behavior likely associated with corrosion and product-related effects.Freq/Hz: 2.153e+4, Z'/ohm: 5.711e+0, Z"/ohm: -5.909e-1, Z/ohm: 5.741e+0, Phase/deg: -5.9The impedance magnitude (Z/ohm) keeps increasing, reflecting ongoing resistance growth.The negative phase angle intensifies, suggesting significant inductive behavior consistent with complex corrosion processes.Freq/Hz: 1.777e+4, Z'/ohm: 5.775e+0, Z"/ohm: -7.046e-1, Z/ohm: 5.818e+0, Phase/deg: -7.0The impedance magnitude (Z/ohm) continues to rise, indicating higher resistance.The substantial negative phase angle suggests pronounced inductive behavior, possibly linked to advanced corrosion processes and changes in the material's surface properties.

This pattern continues for the rest of the data points. The increasing impedance magnitudes and the deepening negative phase angles indicate a transition from capacitive to inductive behavior, likely due to the growth of corrosion products and changes in the material's electrochemical behavior. These observations are consistent with the typical behavior of corroding materials as they are exposed to a corrosive environment over time.

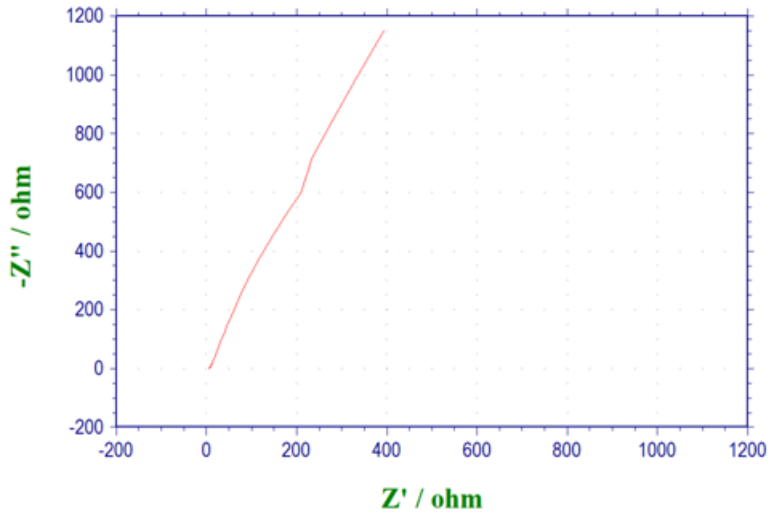

Figur 3: ranndle circuit diagram

The impedance data you provided corresponds to a frequency range from 1 Hz (low frequency) to 100,000 Hz (high frequency) with an amplitude of 0.005 V. This data can be used to construct an

impedance diagram in the context of a Randles equivalent circuit, which is a common model used in electrochemical impedance spectroscopy (EIS) to interpret the impedance response of electrochemical systems.

The Randles circuit consists of several components that represent different electrochemical processes occurring at the material-electrolyte interface. The components typically include a solution resistance (Rs), a charge transfer resistance (Rct), and a Warburg impedance (Zw) to account for diffusion-controlled processes.

Here's how the data you provided might be interpreted using the Randles circuit:At High Frequency (1e+5 Hz):At high frequencies, the impedance response is dominated by the solution resistance (Rs) due to the limited time available for other processes to contribute significantly.The Rs value corresponds to the real part of the impedance at this frequency.At Low Frequency (1 Hz):At low frequencies, the impedance response is influenced by both the charge transfer resistance (Rct) and the Warburg impedance (Zw).The Rct represents the resistance associated with the charge transfer process at the material-electrolyte interface. As frequency decreases, this resistance becomes more significant, leading to an increase in impedance magnitude.The Warburg impedance (Zw) accounts for diffusion-limited processes. As the frequency decreases, the Warburg impedance becomes more dominant, leading to an increase in impedance magnitude. The negative imaginary component of the Warburg impedance reflects the gradual decrease in impedance phase angle (more inductive behavior).

In an impedance diagram, the impedance magnitude (|Z|) is plotted on the vertical axis, and the phase angle (θ) is plotted on the horizontal axis. As frequency increases, the impedance magnitude decreases, and the phase angle becomes more resistive (closer to 0°). As frequency decreases, the impedance magnitude increases, and the phase angle becomes more inductive (closer to -90°).

In your case, the impedance diagram based on the Randles circuit might show a semicircular Nyquist plot at high frequencies, corresponding to the solution resistance (Rs). As frequency decreases, the Nyquist plot transitions into a straight line with an angle close to -45°, indicating the presence of charge transfer resistance (Rct) and Warburg diffusion processes (Zw).

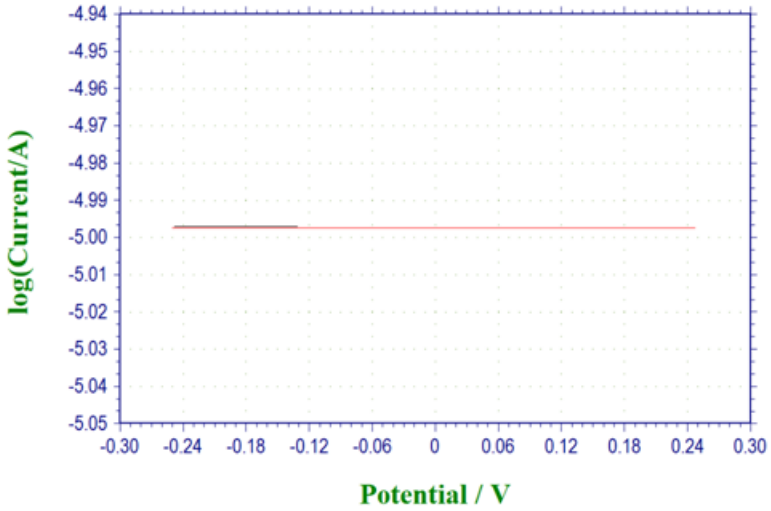

Figure 4: tafel plot

Let's break down the parameters you've provided and explain their significance with the specific values you've mentioned.Initial Voltage (V_init): -0.25 VThis is the starting potential of the cyclic voltammetry experiment. It represents the initial voltage at which the scan begins.Final Voltage (V_final): 0.25 VThis is the ending potential of the cyclic voltammetry experiment. It represents the maximum potential to which the scan is carried out.Segment 1 Hold Time: 0 secondsIn cyclic voltammetry, there are often hold times at specific potentials to allow the system to reach steady-state conditions before starting the next scan segment. In this case, there is no hold time during the first segment, meaning that the scan transitions immediately from the initial voltage to the final voltage.Scan Rate: 0.001 V/sThe scan rate determines how quickly the voltage is changed during the cyclic voltammetry scan. A scan rate of 0.001 V/s means that the potential will change by 0.001 V every second.Quit Time: 2 secondsThis is the total time for which the cyclic

voltammetry experiment will run, including all scan segments and hold times.Anodic Interval Log Step (ano int log s): -4.997This parameter likely represents the logarithmic step size for the anodic scan direction. It indicates that the scan will take steps in the anodic direction with a logarithmic spacing of 10^(-4.997).Corresponding Current (i_a): 1.004e-005his is the recorded current value at the specific potential of interest during the experiment.

Now, let's put these parameters together and explain the experiment based on the provided values:

The cyclic voltammetry experiment starts at an initial potential of -0.25 V and quickly scans towards the final potential of 0.25 V at a scan rate of 0.001 V/s. There is no hold time during the first segment. The quit time for the entire experiment is set to 2 seconds.The anodic scan direction takes steps with a logarithmic spacing of 10^(-4.997) between potential values. At a particular potential of interest, the recorded anodic current is 1.004e-005 Amps.The experiment involves applying a voltage sweep between the initial and final potentials and measuring the resulting current response. The anodic scan will show how the current changes as the potential increases. The logarithmic step size indicates that the scan will cover a wide range of potentials with smaller steps at higher potentials.The recorded current value of 1.004e-005 Amps at a specific potential provides information about the electrochemical reactions occurring at that potential. This can be used to analyze redox processes, oxidation or reduction reactions, and the behavior of the electrochemical system under study.

CONCLUSION

The electroplating solution designed for Ni-Mo coating is a carefully composed mixture of specific components that contribute to the controlled deposition of a Ni-Mo alloy coating with tailored properties. Nickel sulfate (NiSO4) serves as the primary source of nickel ions, while molybdenum sulfate (MoSO4) introduces molybdenum ions into the solution, forming the Ni-Mo alloy. Sodium hydroxide (NaOH) adjusts the pH to around 4, providing optimal electroplating conditions. Additives, such as brighteners and leveling agents, enhance coating quality as recommended. Water is added to adjust volume and concentration accurately.

Analyzing XRD data, lattice spacing (d) and average crystallite size (D) were calculated using Bragg's Law and Scherrer equation, respectively, based on provided 2-theta angles and FWHM values. The impedance data indicates changing electrochemical behavior over a frequency range, suggesting a transition from capacitive to inductive behavior due to corrosion-related processes.

The provided parameters for cyclic voltammetry were interpreted. The experiment involves voltage scanning from an initial to a final potential at a specified scan rate, with anodic intervals defined logarithmically. Recorded current values at specific potentials provide insights into electrochemical reactions occurring within the system.

Reference:

1. Optimizing Electrodeposition Parameters For Ni-Mo Composite Coatings: A Study, Corrosion Resistance And Surface Morphology With Nanoparticle Incorporation Purshotham P. Katti*1, Dr. Praveen B.M2 doi: 10.48047/ecb/2022.11.11.232022.09/08/2023
2. "Comprehensive Analysis Of Corrosion Possibilities In Aircraft: A Multi-Dimensional Examination Of Corrosion Types, Solutions, Metal Recommendations, Identification And Testing Methods" Purshotham.P.Katti* Dr.Praveen B.M*2 doi:10.48047/ecb/2023.12.10.1872023.14/08/2023
3. Corrosion-Resistant Metalnanoparticle Composite Coatings For Industrial Applications: Effect Of Niso4, Nicl2, Mo, Nh4cl, And H3bo3 Concentrations On Nano Particle Concentration Purshotham P. Katti*1, Dr. Praveen B.M2 doi: 10.48047/ecb/2022.11.12.0152022.12/08/2023
4. A Molybdenum Coating on Mild Steel: Preparation, Characterization, and Electrochemical Preparation Purshotham. P. Katti, B. M. Praveen, SSRG - IJMSE, **Volume** 9, **Year** 2023, **Pages** 13-21
5. Recent Advances in Ni-Mo Electroplating with Nano Particle Bath Additives: A Literature Survey Purshotham. P. Katti, B. M. Praveen, SSRG International Journal of Material Science and Engineering, **Volume** 9, **Year** 2023, **Pages** 22-35
6. "Electrical energy harvesting in aircraft by using carbon fiber battery. "Purshotham. P. Katti, Abhinand , Amaresh, Dibu, shekar prasad journal of Emerging Technologies and Innovative Research, **Volume** 6, **Year** 2019, **Pages** 437-449
7. Alimadadi, H et al., “Electrodeposition of Molybdenum on Steel Substrates: Study of

Surface Morphology, Adhesion, and Corrosion Resistance," Surface Engineering, vol. 32, no. 6, pp. 427-433, 2016.
8. Singh, D. K., Yadav, T. P, and Yadav, R. M, "A Review on Electrodeposition of Molybdenum and Molybdenum Alloys," Journal of Materials Science: Materials in Electronics, vol. 27, no. 9, pp. 9502-9512, 2016.
9. Aravindan, S., Madhavan, J, and Kamaraj, P, "Molybdenum Coatings on Steel Substrate: A Review," Surface Engineering, vol. 35, no. 7, pp. 557-567, 2016.
10. Alimadadi, H et al., "Investigation of the Effect of Current Density and Plating Time on the Properties of Electrodeposited Molybdenum on Steel Substrates," Surface Engineering, vol. 33, no. 9, pp. 687-692, 2017.
11. Song, M. H., Oh, J. W., and Han, K. S, "Electrodeposition of Molybdenum on Steel Substrates Using Ionic Liquids as Electrolytes," Journal of the Korean Physical Society, vol. 68, no. 2, pp. 252-257, 20167
12. Wu, W. J., Zhang, X. J., and Wang, Y. S, "Electrodeposition of Molybdenum on Steel Substrate from Deep Eutectic Solvent-Based Electrolyte," Transactions of Nonferrous Metals Society of China, vol. 29, no. 1, pp. 44-53, 2019.
13. Aravindan, S, and Kamaraj. P, "Electrodeposition of Molybdenum on Mild Steel Substrate: Optimization of Process Parameters Using Response Surface Methodology," Transactions of Nonferrous Metals Society of China, vol. 27, no. 5, pp. 1025-1032, 2017.
14. Du, C., Yan, Y., Wang, S., and Liu, Q., "Electrodeposition of Molybdenum Coating on Steel in Ionic Liquids," Journal of Materials Science: Materials in Electronics, vol. 31, no. 1, pp. 11-16
15. Li, Y., and Yang, W, "Study of Electrodeposition of Molybdenum on Steel Substrate in Ionic Liquid," Journal of Physics: Conference Series, vol. 832, no. 1, pp. 012007, 2017.
16. Liu, C., Li, Y., and Yang, W, "Electrodeposition of Molybdenum on Steel Substrate in Room Temperature Ionic Liquid [BMIM][TF2N]," International Journal of Electrochemical Science, vol. 13, no. 11, pp. 11389-11399, 2018
17. Zhan, H., Zhang, Y., Zhang, J., and Wang, Y, "Electrodeposition of Molybdenum Coating on Steel in 1-Butyl-3-Methylimidazolium Tetrafluoroborate," Journal of Materials
18. K.R. Sriraman, S. Ganesh Sundara Raman, and S.K. Seshadri, "Corrosion Behaviour of Electrodeposited Nanocrystalline Ni–W and Ni– Fe–W Alloys," Materials Science and Engineering: A, vol. 460–461, pp. 39–45, 2007.
19. T.N.Guma, and James A.Abu, "A Field Study of Outdoor Atmospheric Corrosion Rates of Mild Steel Around Kaduna Metropolis," SSRG International Journal of Mechanical Engineering, vol. 5, no. 11, pp. 7-21, 2018
20. Tetsuya Akiyama, and Hisaaki Fukushima, "Recent Study on the Iron-Group Metal Alloy," ISIJ International, vol. 32, no. 7, pp. 787– 798, 1992
21. M Naka, K Hashimoto, and T Masumoto, "High Corrosion Resistance of Amorphous Fe–Mo and Fe–W Alloys in HCL," Journal of Non-Crystalline Solids, vol. 29, no. 1, pp. 61–